JOURNAL OF GEOPHYSICAL RESEARCH, VOL. 106, NO. D23, PAGES 32,555–32,569, DECEMBER 16, 2001

Dust and pollution transport on global scales: Aerosol measurements and model predictions

A.D. Clarke,[1] W.G. Collins,[2] P.J. Rasch,[2] V.N. Kapustin,[1]
K. Moore,[1] S. Howell,[1] and H.E. Fuelberg,[3]

Abstract. Vertical profiles of aerosol and gas phase species were measured on flights near Hawaii on April 9 and 10, 1999, during NASA's Pacific Exploratory Mission (PEM) Tropics B program. These measurements characterized aerosol microphysics, inferred chemistry, optical properties, and gases in several extensive dust and pollution plumes, also detected by satellites, which had 10,000-km trajectories back to sources in Asia. Size-resolved measurements indicative of aerosol sulfate, black carbon, dust, light scattering, and absorption allowed determination of their concentrations and contributions to column aerosol optical depth. A new Chemical Transport Model (CTM) that includes aerosol, meteorological fields, dynamics, gas and particle source emissions, a chemistry component (MATCH), and assimilated satellite data was used to predict aerosol and gas concentrations and the aerosol optical effects along our flight path. Flight measurements confirmed the "river-like" plume structures predicted by the CTM and showed close agreement with the predicted contributions of dust and sulfate to aerosol concentrations and optical properties for this global-scale transport path. Consistency between satellite, model and in situ assessment of aerosol optical depth was found, with noted exceptions, within ~25%. Both observations and model results confirmed that this aerosol was being entrained into the marine boundary layer between Hawaii and California where it can be expected to modify the type and concentration of cloud condensation nuclei in ways that may alter properties of low-level clouds. These observations document the significance and complexity of long-range aerosol transport and highlight the potential of emerging CTM models to extend observational data and address related issues on global scales.

1. Introduction

In the past decade, increased interest in atmospheric particles (aerosol) has been generated in response to concerns over possible climate effects through their direct perturbation to the radiation budget (direct effect) [*Charlson et al.*, 1992] or through changing the cloud microphysics and cloud lifetime [*Albrecht*, 1989] or their reflectivity (indirect effect) [*Kaufman and Fraser*, 1997]. More recently, satellite observations of rainfall suppression in clouds caused by combustion aerosol raise concerns over significant impacts on the hydrologic cycle [*Rosenfeld*, 1999, 2000]. Related effects due to the highly absorbing soot component appear to include the "burning off" of cloud tops in shallow cumulus that can result in enhanced regional heating in polluted air masses [*Ackerman et al.*, 2000]. Other active topics in aerosol research include their role in geochemical cycles and in the sulfur, nitrogen, and carbon budgets [*Galloway et al.*, 1984], biomass burning, iron "fertilization" (dust input) of ocean surface waters [*Duce and Tindale*, 1991; *Martin and Gordon*, 1987; *Measures and Vink*, 2000], desertification and dust transport [*Prospero et al.*, 1999], etc. Recent rapid developments in chemical transport models [*Tegen et al.*, 1997) and new satellite capabilities that use or interpret upwelling radiance [*King et al.*, 1999] are also driving the need to understand aerosol sources and their chemical and radiative properties on global scales. These interests have led to a number of large focused experiments in recent years (e.g., ACE-1, ACE-2, TARFOX, INDOEX) that have attempted to address various issues by investigating aerosol chemistry, physics, and their optical effects in diverse regions.

The NASA Pacific Exploratory Mission (PEM) experiments are part of the Global Tropospheric Experiment (GTE) that has recently fielded three major gas and aerosol aircraft experiments throughout the Pacific troposphere. The PEM results (http://www-gte.larc.nasa.gov/gte_miss.htm) include data from pristine and polluted regions and have focused on the characterization and understanding fundamental chemical processes in the troposphere. The latest experiment, PEM Tropics B, took place in March and April 1999 and examined fundamental gas and aerosol processes in the South and Equatorial Pacific regions. On the return leg to Hawaii on April 9, 1999, at the end of the campaign, we detected significant dust and pollution aerosol during our approach to Hawaii. Meteorology and satellite data (AVHRR, SeaWiFS) suggested active aerosol transport over the North Pacific from Asia. Consequently, we adopted a measurement strategy on the transit flight from Hawaii to California on April 10, 1999, that optimized sampling of gas and aerosol species through a

[1]School of Ocean and Earth Science and Technology, University of Hawaii, Honolulu, Hawaii.
[2]National Center for Atmospheric Research, Boulder, Colorado.
[3]Department of Meteorology, Florida State University, Tallahassee, Florida.

Paper number 2000JD900842.
0148-0227/01/2000JD900842$09.00

combination of vertical profiles and short horizontal legs. This approach was very successful, and we were able to investigate dust and pollution plume properties with state of the art instrumentation after ~10,000 km of transport from Asia. Here we focus upon the aerosol measurements and related aerosol model products for this flight.

In recent years, new satellite (AVHRR, SeaWiFS) and model products (MATCH [*Rasch et al.*, 1997], NAAPS-Navy Aerosol Analysis and Prediction System, see http://www.nrlmry.navy.mil/aerosol/Docs/globaer_model.html) have emerged that help resolve contributions to the remote troposphere aerosol and gas concentrations. These are run in an analytical mode and more recently in a predictive mode [*Collins et al.*, 2001]. These also use procedures to estimate associated optical effects. Some large experiments (ACE-2, TARFOX, INDOEX) have assembled the tools and data to challenge these model products but they have all operated within about 1000 km of the sources or less [*Collins et al.*, 2001]. These near-source measurements make aircraft interception of elevated concentrations more predictable and more readily detectable. However, global environmental issues require that these products ultimately be compared and interpreted after atmospheric processes have acted over far greater distances. The opportunistic interception of a major continental plume after 10,000 km of transport with our PEM Tropics B ferry flight provides a unique data set with which to characterize such plumes and explore both model and satellite interpretations. These are not presented here in terms of a validation of model or satellite products since the flight plan for the experiment was not optimized for that purpose. However, these data provide a basis for evaluation of model performance in terms of extended global-scale aerosol transport. The observations presented here are encouraging for the potential application of these new CTM models to global issues involving aerosol effects, chemical transport, and satellite interpretation.

2. Aerosol Measurements

Aerosol measurements during PEM Tropics B aboard the NASA P3 included condensation nucleus (CN) counters measuring CN concentrations at ambient and 300°C. The latter refractory CN (RCN) are typically soot, dust, and sea-salt and are all surface derived and the ratio of RCN to CN provides a gauge of the surface derived contribution to CN. A laser optical particle counter (OPC) sized particles from 0.1 to 4.0 μm, and a differential mobility analyzer (DMA) provided sizing of "dry" particles from 0.01 to 0.28 μm. Both instruments were heated to three temperatures chosen to reveal characteristics of sulfate and refractory aerosol based upon size resolved volatility [*Clarke*, 1991]. Sizes were accumulated typically over periods of 1-3 min. A Gerber (PVM 100) probe was used on the wing to size larger ambient particles including cloud water droplets to yield liquid water content.

Light scattering at three wavelengths (450, 550, 700 nm, TSI 3070 integrating nephelometer) and light absorption (Radiance Research, PSAP) established aerosol scattering and absorption coefficients. When these two optical properties are added, they define the extinction coefficient, and the ratio of the scattering coefficient to the extinction coefficient also defines the aerosol single scatter albedo $\bar{\omega}$. This is an important parameter for modeling aerosol radiative effects [*Quinn et al.*, 1995] and is independent of concentration. An impactor with a 1-μm aerodynamic cutoff size periodically removed large particles from the airstream to establish their contribution to the scattering coefficient and $\bar{\omega}$. This provided separate assessment of the scattering caused by total and submicrometer particles. This aerodynamic cutoff size for unit density spheres will be nearer 0.75-μm geometric size for the dust encountered here.

Particle size and volatility can be used to assess aerosol mass and infer chemical composition needed to estimate refractive index and optical properties [*Clarke et al.*, 1996]. These estimates can be compared to measured dry optical properties as a test of consistency in the calculations and approach. Further allowance for aerosol water uptake at ambient RH based upon inferred chemistry is needed to determine ambient aerosol extinction and ambient optical depth [*Clarke et al.*, 1996; *Quinn et al.*, 1995]. The resulting ambient characteristics can then be linked to CTM model parameters and/or to upwelling radiance retrieved from satellite. In this fashion model products and satellite retrievals can be compared to in situ data.

3. Model Characteristics

Later we will compare our PEM Tropics B data with a model and data assimilation procedure described in *Collins et al.* [2001] and *Rasch et al.* [2001]. The assimilation procedure combines satellite measurements and an aerosol simulation using a global chemical transport model called MATCH [*Rasch et al.*, 1997]. Retrievals of aerosol optical depth from AVHRR satellite imagery [*Stowe et al.*, 1997] is used to adjust the aerosol fields predicted by the model through an assimilation technique. Evolution of the aerosol field is driven by meteorological fields from a numerical forecast-center product. This procedure produces a global aerosol data set consistent with the measurements "regular" in space and time. Where there are no satellite measurements, the model aerosols are a combination of assimilated values introduced into the data set upstream in space and time with the values the model would predict in the absence of any observations. The estimate is relevant to a precise place and time because the meteorology is constrained to agree with observations. The procedure can be used to produce an aerosol "forecast" where aerosol distributions are predicted some short time into the future (the meteorological specification comes from a combination of operational numerical weather prediction center analysis and forecast products). Alternately, it can generate an "aerosol analysis" where the distributions represent an optimal estimate for some period in the present or past.

The assimilation procedure produces estimates for four aerosol species: dust, carbonaceous (elemental and organic), sulfate, and sea salt. Dust is resolved into four size categories for particles 0.01 to 1, 1 to 10, 10 to 20, and 20 to 50 μm in diameter. The dust is mobilized as a function of surface wind speed and surface properties (soil type, vegetation, and land use). The carbonaceous and sulfate aerosols use prescribed climatological emission estimates [*Smith et al.*, 2001; *Liousse et al.*, 1997; *Penner et al.*, 1993; *Cooke and Wilson*, 1996]. Sea-salt concentrations are diagnosed as a function of wind speed and height above the surface [*Blanchard and Woodcock*, 1980]. The model outputs global three-dimensional fields of aerosol mixing ratios for each species along with the

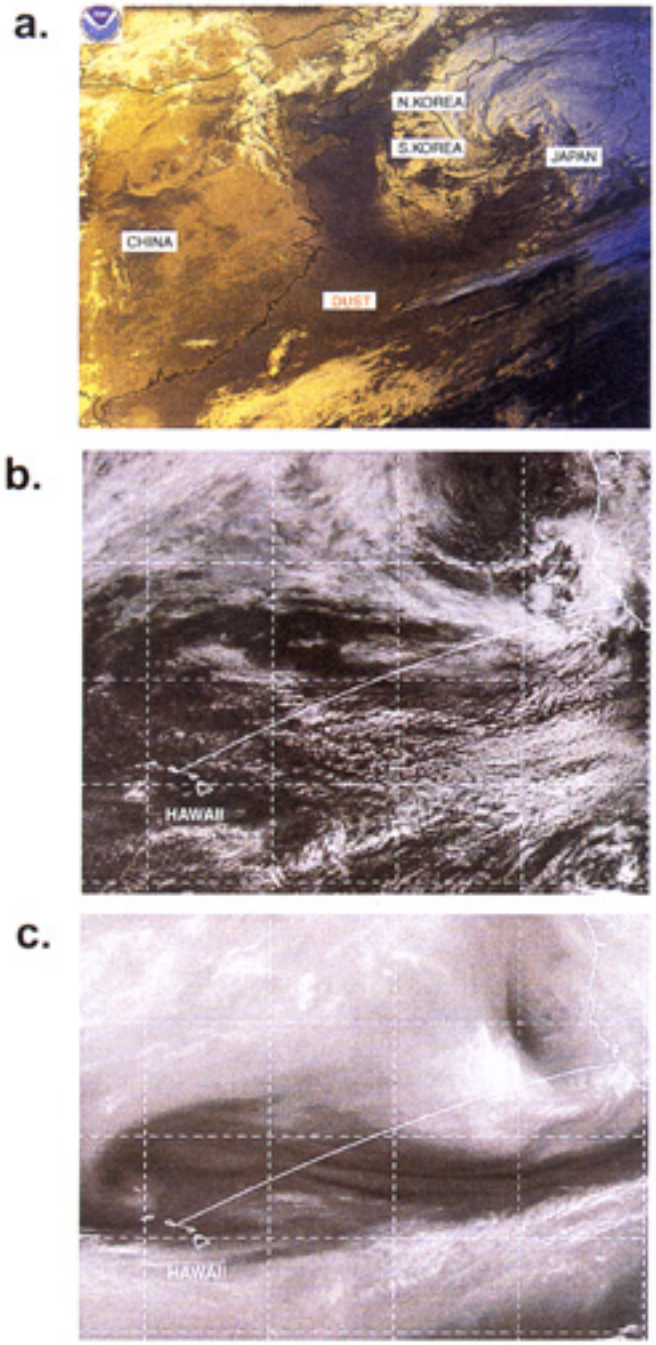

Plate 1. Satellite images associated with flight 18, April 10, 1999. (a) SeaWiFS image for April 6 reveals huge arc of dust swept out from China and associated cyclonic activity over Japan that is mixing in polluted air from Korea and Japan before heading across North Pacific to region we flew in on April 10. (b) GOES visible image of medium high clouds to north and low California stratocumulus to south with flight track included. (c) GOES water vapor image showing large dry area early in flight where dry dust layers were encountered.

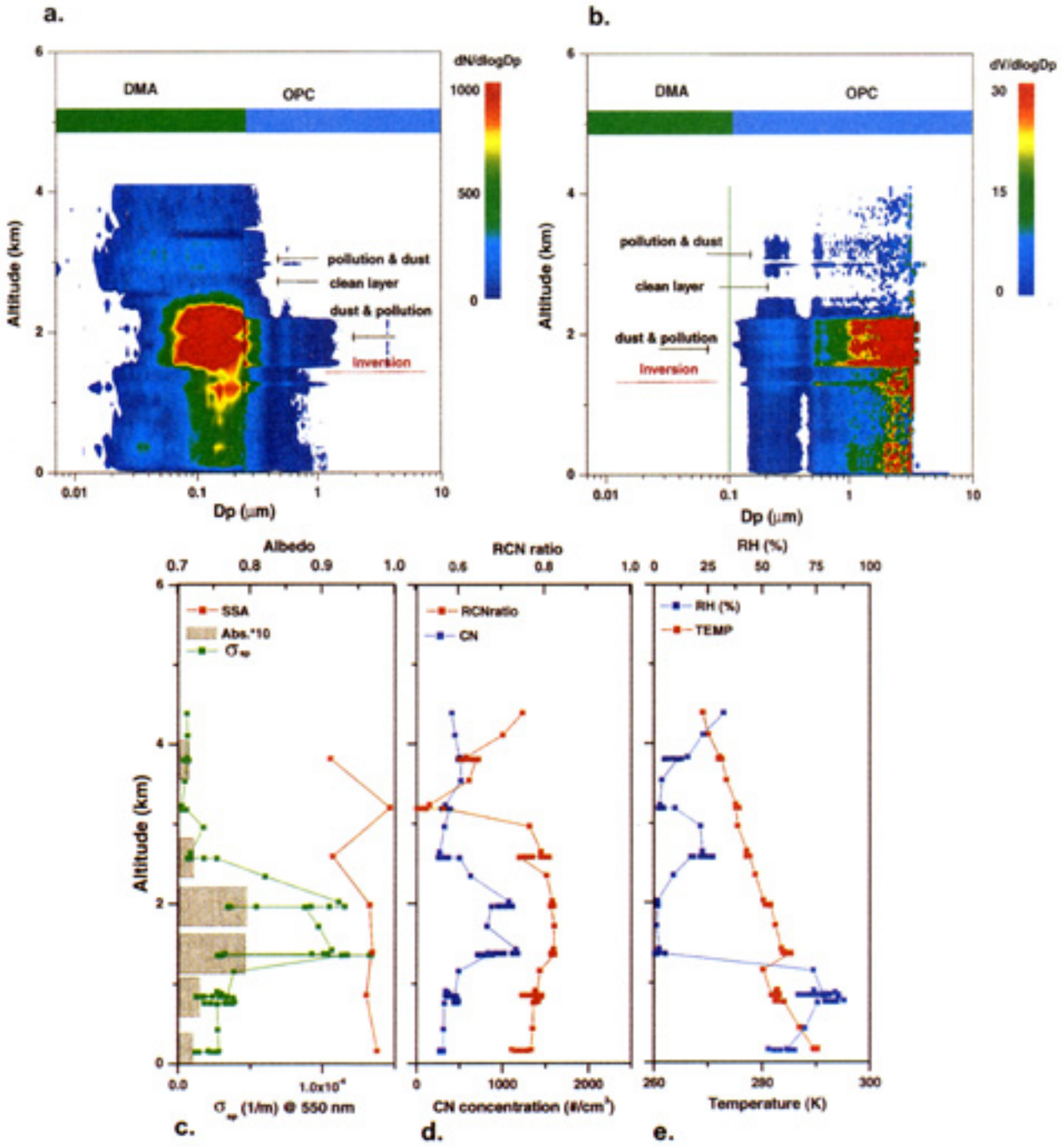

Plate 2. Vertical profiles of color coded size distributions for (a) number concentrations [particles/cm^3] and (b) volume concentrations [$\mu m^3/cm^3$] for the stepped ascent in the middle of flight 18, revealing that both submicrometer pollution (Dp ~ 0.15 μm) and coarse particle dust (Dp ~ 2+ μm) are enhanced in main plume. Higher layers are interspersed with clean layers. (c) Vertical profiles of aerosol light scattering, light absorption, and the associated single scatter albedo. Drops in scattering to low values are due to removal of coarse particles when the nephelometer impactor is in place. (d) The high stable RCN ratio below 3 km suggests continental influence is present to the surface. Near 3 km the low scattering, low RCN ratio, and high single scatter albedo indicate very clean air separating lower and upper layers from the lower. SO_2 is also elevated in the plume. (e) Temperature and relative humidity (RH) reveal locations of inversions and dry layers aloft where peak aerosol layers occur.

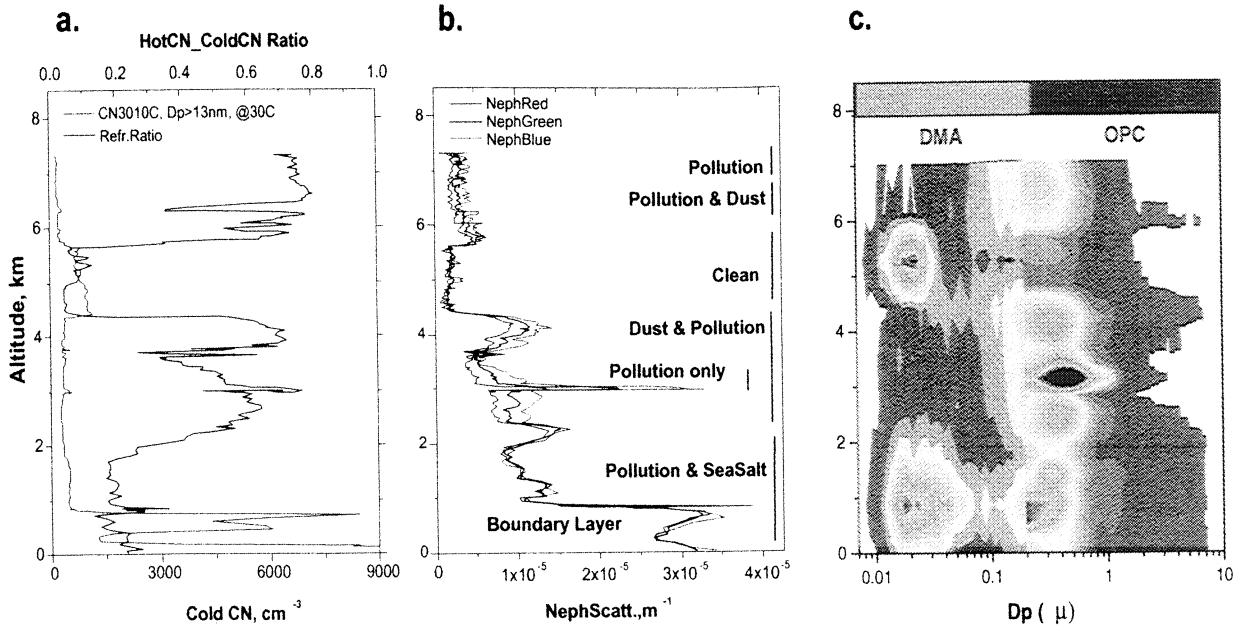

Figure 1. (a) Vertical profiles for the gradual descent into Hawaii from the south on April 9, 2000. The low condensation nucleus (CN) and high refractory CN (RCN) ratio in dry air (not indicated) are characteristic of continental aerosol often associated with dust events. The low RCN ratio and elevated CN near 5 km are typical of clean cloud processed air. (b) Aerosol light scattering at (450, 550, 700 nm) reveal fluctuations in aerosol light scattering related to aerosol mass and the changes in wavelength dependence indicates variations in particle size associated with different layers. (c) Altitude plot of aerosol concentration (gray scale) versus particle size. Note coarse dust aerosol near 4.5 and 6.5 km with clean air from 5 to 6 km.

column-integrated aerosol optical depth for each species at 6-hour intervals.

Biases in the aerosol estimates can be attributed to errors in emission inventories, errors in the meteorological specifications, and errors in the model transport and removal processes. These can be examined in a methodical fashion, but this assessment is extremely difficult to perform quantitatively, and it has not yet been done. The assimilation procedure acts to reduce the bias introduced by these errors by adjusting the distributions in an optimal way to agree with observations. Because the observable (currently the aerosol optical depth reported at a single wavelength) used in the assimilation represents a vertically integrated quantity, the adjustment procedure is significantly underdetermined.

4. Observations

PEM Tropics B flight 17 originated in Tahiti on April 9 and ended in Hawaii. Data from this flight provided our first indication that active aerosol transport was taking place from Asia over the Pacific. Figures 1a and 1b show data from this gradual descent profile into Hawaii from 7.4 km. Included are the aerosol light scattering coefficient, the condensation nuclei (CN) concentration, the ratio of refractory CN (RCN) to total CN (RCN ratio) remaining after heating to 300°C, and the observed size distribution (shaded for concentrations). The low CN values and high values of the RCN ratio aloft are indicative of aged pollution and dust aerosol [*Clarke et al.*, 1993]. The uncommonly high CN and low RCN ratio values (high fraction of volatile CN) near the surface in the marine boundary layer (MBL) are dominated by volatile sulfates from the Kiluaea volcano that is active ~200 kilometers upwind of this location.

Above 1 km the overlying layers of pollution, dust, and clean air are interspersed and evident in the size distributions where dust particles larger than a micrometer are apparent (Figure 1c). Near 3 km these distributions show the submicrometer aerosol enhanced relative to coarse dust, as expected for a pollution aerosol. However, the somewhat elevated number of CN near 5 km and low light scattering values reveal a layer of smaller particles with low mass. The corresponding low RCN ratio indicates that these are more volatile and the higher relative humidity is consistent with them being a naturally produced aerosol associated with cloud outflow and natural sulfur chemistry [*Clarke et al.*, 1998,1999]. These layer differences are also consistent with 10-day back trajectories that show this clean layer has moved only slowly from over the central Pacific, while the rapidly moving layers above (6.5 km) and below it (4 km) pass over India and Asia respectively (Figure 2).

This initial evidence (flight 17) for long-range transport of continental aerosol dominating layering in the tropical North Pacific prompted our examination of satellite imagery from a few days earlier. These indicated major dust and pollution outbreaks active from Asia (Plate 1a) and motivated deliberate efforts to systematically profile the atmosphere the following day (flight 18) on the transect to California. Visible GOES imagery (Plate 1b) for that day includes our flight track and shows various cloud fields over the region with higher clouds to the north and low level stratocumulus predominately to the south. Water vapor imagery (Plate 1c) also shows a band of drier air ~10° wide extending from Hawaii to California and encountered during the first half of the flight.

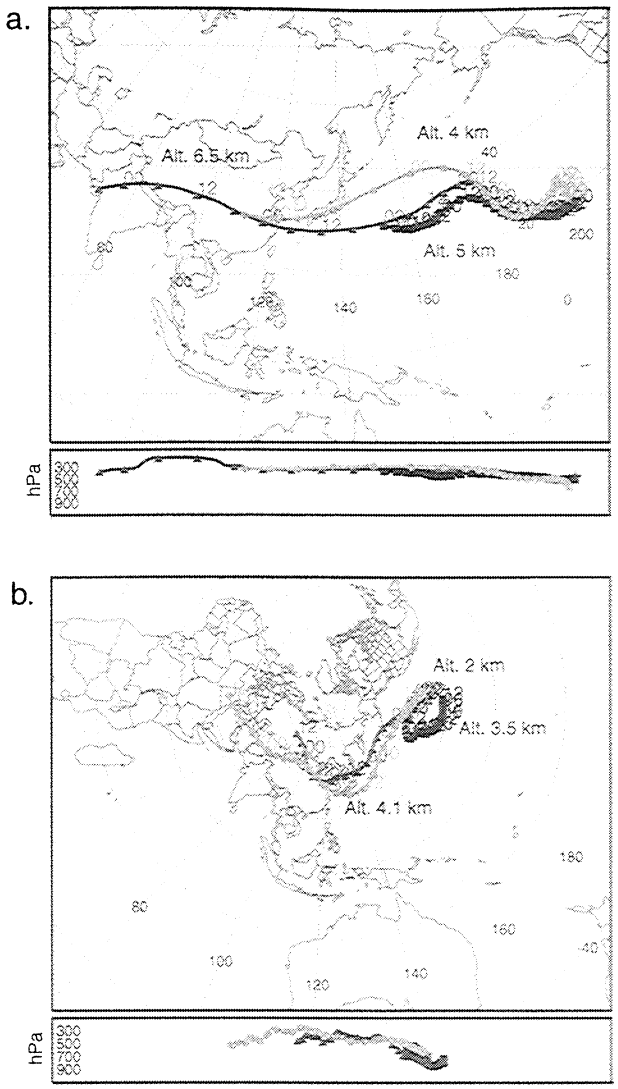

Figure 2. Ten-day HYSPLIT back trajectories for three altitudes (indicated) during profiles for flights 17 and 18, suggesting sources for continental layers from Asia, India, or Africa. Shorter trajectories at (a) 5 and (b) 3.5 km are for "clean" layers that have lower wind speeds and remain confined to Pacific Ocean region.

Plates 2a-f show measurements of gas and aerosol properties for our stepped ascent profile midway between Hawaii and California during flight 18. The associated aerosol size distributions shown in Plates 2a and 2b are a combination of DMA and OPC data for diameters (Dp) between 0.01 and ~4 μm and reveal characteristic differences in each of the regions indicated. Both number distributions dominated by the DMA data and volume distributions dominated by the OPC data are separately indicated in the two panels. Coarse particles with diameters larger than 1 μm are generally dust or sea salt, while smaller sizes are generally dominated by sulfate, organic species, and black carbon (BC). The sharp truncation of particles larger than ~3 μm often evident in the volume distributions is a consequence of the OPC electronics used here, but it implies more coarse particles are present at even larger sizes.

Plates 2a and 2b reveal a pronounced layer near 2 km with large numbers of both coarse and fine aerosol present at low relative humidity (RH) (<10%) (Plate 2f). This is consistent with our typical observations of coarse particles in dry "dust" layers aloft. The surface layer also has coarse and fine aerosol but at much lower concentrations, and it has the high RH characteristic of the MBL. However, it is important to note that the highest accumulation mode number below the inversion is evident near 1.2 km (Plate 2a) with concentrations decreasing toward the surface, indicating a source aloft. The coarse aerosol at this altitude (Plate 2b) also decreases to reach a minimum near 0.8 km. However, the increase in coarse particle volume but not in fine particle number below 0.8 km is what would be expected for an additional near surface source of coarse sea salt. These observations clearly indicate that the pollution/dust layer above the inversion is being entrained and mixed down into the MBL. This is also evident in the MBL values for light absorption being higher near 1 km than the surface (Plate 2c). Since both fine and coarse modes should be entrained together, the relative fraction of coarse and fine plume concentrations mixed into the MBL should be similar to the light absorbing aerosol (about 30%).

The pollution/dust layer near 3.0 km has an intermediate RH value near 25%, and all particle sizes show low concentrations. Above that altitude, fine particles start to increase again in another dry layer but with a lower concentrations of coarse particles than the 2-km layer. Air above 4 km has moderate RH, consistent with climbing into a moderate RH, consistent with climbing into a higher water vapor region (Plate 1c), and the higher CN. However, the lower light scattering reflects a transition to much smaller particles. Even so, the increasing RCN ratio and detectable absorption above 3.5 km indicate a combustion aerosol. This is in contrast with the "clean" air near 5 km with low RCN ratio seen on flight 17 the previous day (Plate 2e).

5. Plume Microphysics and Optics

This vertical structure is also expressed in the aerosol optical properties including the light scattering coefficient, absorption coefficient, and single scatter albedo shown in Plate 2c. The periodic sharp drops in scattering coefficient evident at various altitudes are the effect of using the impactor to remove large particles in the nephelometer during a horizontal "stair-step" leg. This procedure confirms that at least 60% of the light scattering in the main plume is due to coarse particle dust larger than 1 μm. However, the aerosol light absorption coefficient is dominated by the BC [*Clarke and Charlson*, 1985; *Clarke*, 1989] originating from combustion processes. The light-absorption values shown here are averages over the horizontal stepped legs. This avoids the artifact problem that can influence this measurement during continuous vertical motions [*Clarke et al.*, 1997].

Hence, although BC is present in the surface layer, it is far more concentrated in the plume layer from 1.2 to 2.5 km. The clean region of low BC values from 2.7 to 3.2 km separates this lower plume from the less pronounced upper layer between 3.3 and 4.5+ km. The 1-2 and 4 km layers are different plumes and possibly different sources as evident in the differences in single scatter albedo $\bar{\omega}$, an intensive (concentration independent) property of the aerosol (Plate 2c). This is due in part to the relative depletion of dust in the upper plume with its higher scattering and lower absorption. Also, note that $\bar{\omega}$ in the surface layer is near 0.97 and higher than aloft, a result

consistent with both lower absorption in the MBL and increased scattering by nonabsorbing coarse sea salt. The intervening clean layer near 3 km has $\bar{\omega}$ greater than 0.99 with no detectable absorption. Thus in situ measurements of properties in the surface layer reveal little about the aerosol properties of the column above.

Back trajectories (Figure 2b) also suggest different Asian source regions for the two layers, while the10-day trajectory for the intervening clean layer remains over the Pacific and implies influence by tropical convection. Hence this single profile reveals how multiple clean and continentally influenced aerosol layers can coexist over the mid-Pacific and how variable the column physical, chemical, and optical properties can be. In spite of the impression that the major plume character (Plate 1a) is dust-like, the significant submicrometer particle mode, increased CN (Plates 2a and 2b), and elevated light absorption from BC clearly indicate a significant combustion contribution.

This information on aerosol size, inferred composition, and vertical structure is used here to calculate optical properties for comparison to onboard measurements of scattering and absorption. There are recognized uncertainties associated with refractive index, size changes with RH, and coarse particle sampling efficiency of the OPC, etc. that can limit accuracy to ~20% [*Clarke et al.*, 2001). Alternately, actual measured scattering and absorption coefficients (Plate 2c) can be used, after correction for nephelometer truncation error [*Anderson and Ogren*, 1998] and correction for aerosol growth from instrument to ambient RH (S. Howell et al., unpublished manuscript, 2001), to derive ambient extinction coefficients. Both approaches can be integrated over the column to obtain column aerosol optical depth (AOD) for comparison to model AOD or values estimated from satellite data.

Size distributions averaged over the horizontal legs during the stepped ascent are shown in Figure 3a at scales that emphasize the submicrometer accumulation mode and its volatility. These are shown for three temperatures chosen to reveal total dry (20% RH) aerosol (light gray), after removal of low-temperature volatile aerosol like sulfuric acid (gray, 150°C), and after removal of sulfates and organic components (black, 300°C). The dry accumulation mode peak below 0.5 μm and the refractory dust mode above 1 μm are clearly evident. Between 1 and 2 km most residual material remaining at 300°C is in the shallow peak below 0.5 μm and typically includes the absorbing refractory BC (shaded). The lack of change in the volatile component between ambient (light gray) and 150°C (gray) suggests an ammonium bisulfate aerosol [*Clarke*, 1991]. A similar volatile coating on the refractory dust aerosol is apparent between about 0.5 and 1.0 μm. This is consistent with individual particle analysis that has found that 50-80% of dust particles downwind of Beijing were coated with sulfate [*Parungo et al.*, 1995]. This would increase the role of sulfate associated with the dust in addition to the accumulation mode sulfate estimated from submicrometer aerosol volatility.

These dry size and volatility data are used to infer size-dependent composition that allows calculation of scattering and absorption coefficients at 550-nm wavelength for the coarse dust and fine particle sulfate mix below ~0.5 μm. When combined, they provide an extinction coefficient for all size distributions during the ascent. This is integrated over height to get the cumulative optical depth profile for fine (sulfate), coarse (dust), and total aerosol shown in Figure 3b. To do this, we had to alter some particle diameters and refractive indices to reflect the difference between measurement humidity (roughly 20%) and ambient conditions. Particles <0.4 μm were assumed to have properties similar to pollution in INDOEX, with growth factors as measured by *Massling et al.* [2001] and refractive indices as calculated by *Chowdhury et al.* [2001]. Above the boundary layer, the coarse mode (>0.8 μm) was assumed to be dust (no RH growth, refractive index 2.3). Below the inversion at 1.25 km, the coarse mode was probably a mixture of dust and sea salt. Particles between 0.4 and 0.8 μm were treated as a mixture of the fine and coarse modes. To estimate the contribution of dust to the boundary layer aerosol, we assumed that it was entrained into and removed from the boundary layer in the same manner as soot. As mentioned earlier, Figure 2c shows that absorption in the MBL decreases toward the surface along with the fine mode aerosol (Figure 2a). If dust behaved the same way, it made up essentially all of the coarse mode above 400 m and about half of the aerosol below. The balance in the lowest 400 m was assumed to be sea salt with growth in response to increasing humidity calculated from *Tang et al.* [1997].

On the basis of the above procedure and size distributions shown in Figure 3a, the cumulative contribution to AOD during descent for the fine particle (sulfate) mode and the coarse dust mode is shown in Figure 3b. These yield contributions to total column AOD of ~0.018 (fine), 0.110 (coarse), and 0.13 (total). Sea salt in the lower 400 m is estimated to contribute about 0.002 to AOD, probably due to low surface winds in this extended high-pressure region. The sulfate evident on the lower tail of the coarse distribution could effectively double the contribution of sulfate to the AOD and reduce the dust contribution by a similar amount. Hence, for the sake of comparison to model results we argue that the sulfate AOD would be accordingly ~0.036 and the dust ~0.092. The total will be little affected by this reallocation. However, we also found calculated scattering to be ~15% less than we obtained from the integrating nephelometer data. Part of this is due to the upper sizing limit on this OPC of ~4 μm (Plate 2b). Nephelometer values also underestimate actual values due to angular truncation error, particularly for coarse particles. For the dust size ranges evident here these have been found to require a multiplier of ~1.5±0.2 for this nephelometer [*Anderson and Ogren*, 1998]. Hence, our estimated contribution to column optical depth based upon the dust aerosol size distribution and scaled with nephelometer performance to be ~(0.092 × 1.15 × 1.5 = 0.159).

Our resulting best estimate of column optical depth due to the aerosol measured on the profile and described as sulfate is 0.036 and dust+sea salt is 0.162 for a total of ~0.20 with an estimated uncertainty of ~0.03.

These values are consistent with the range of values available for the AVHRR satellite for this day and produced by NOAA-NESDIS [*Stowe et al.*, 1997]. Plate 3 shows the satellite composite data average for this day. However, with limited satellite passes and with limited cloud free areas (see Plate 1b) most of the data on this composite are data contributed from days before and only the sparse clear regions with favorable satellite coverage will reflect new data. Even so, the typical scale of aerosol fields and elevated AOD inferred by the satellite is clearly evident. It is also possible that dust and pollution in dry air such as we measured here (Plate 2) will be

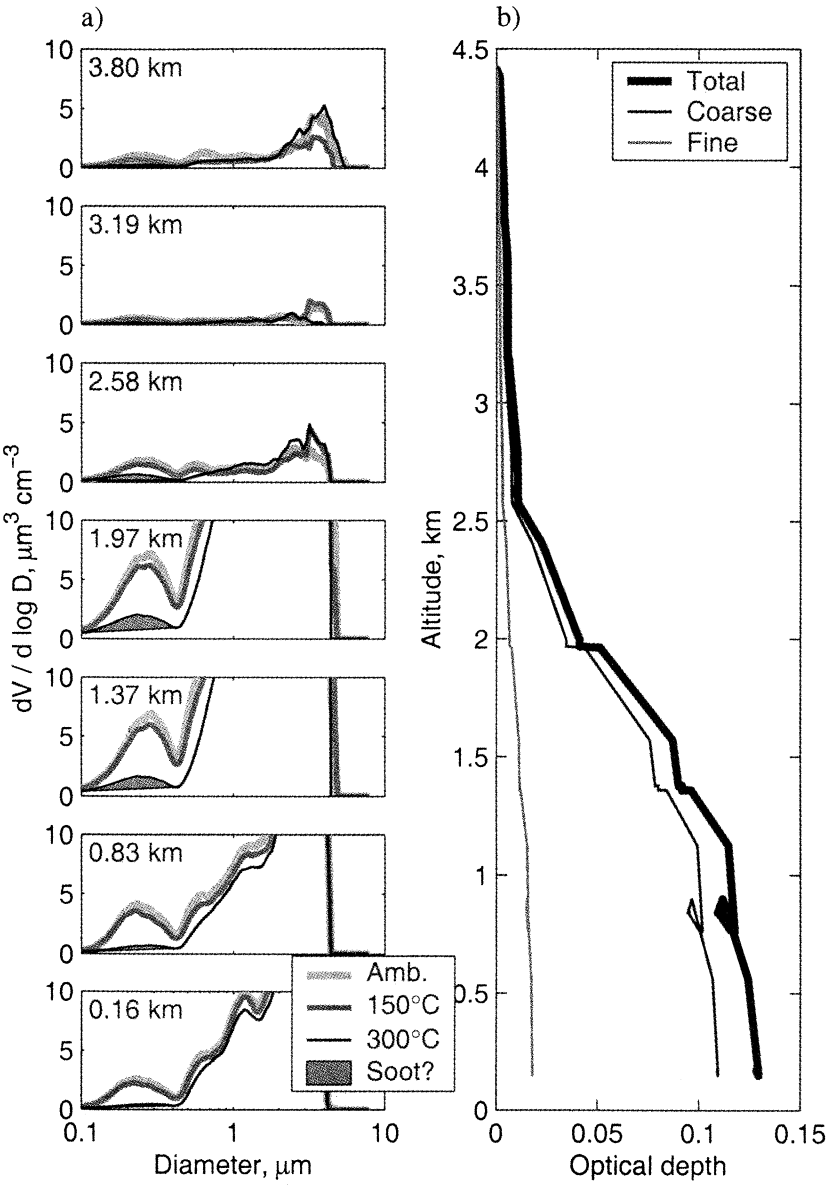

Figure 3. Averaged size distributions for each of the legs on the stepped ascent for flight 18. These are for three temperatures (ambient, 150°C, 300°C) chosen to reveal loss of sulfuric acid (150°C) and sulfate/organics (300°C). The residual shaded 300°C peak is indicative of the refractory soot component. Otherwise, the residual aerosol at 300°C (black curve) is taken to be the dust component. Cumulative optical depth based upon all size distributions is shown in the right hand panel (see text).

the dry air regions that are also more cloud free (see Plates 1b and 1c) and more readily sampled by the AVHRR satellite. This raises the question of a possible bias to optical depths that may be present in cloud free pixels. In any event, the AVHRR optical depths (Plate 3) in the vicinity of our transect suggest a range of 0.15 to 0.25 that encompasses the value from our measurements.

6. Comparison to Model

Before discussing the model results it is important to review some of the model features. The version of MATCH used for these simulations employs NCEP Aviation Analyses/Forecasts for the meteorological specification available every 3 hours. The analyses were interpolated in time to provide a smooth meteorological specification every 30 min (the MATCH time step for this simulation), but there is no real transient information on shorter timescales than every 3 hours.

The model and meteorological fields have 28 levels in the vertical [*Kalnay et al.*, 1996] and the dynamical equations after Fourier transformation are constrained with a horizontal spectral truncation at wavenumber $N = 126$. Therefore the horizontal resolution of the meteorological data and model run is ~90 km at the equator, with the east-west grid spacing decreasing as the cosine of latitude. North near the Aleutians the nominal horizontal resolution is somewhat higher than 90 km in the east-west direction but does not change in the north-south direction. Model layers are also thinner near the surface (surface layer thickness is ~100 m) and gradually increase in

thickness (at 3 km thickness is ~500 m, and at 5 km it is ~1 km). Since the model is integrated globally, no lateral boundary conditions are necessary. The integration is started on February 1, 1999, from initial conditions from a simulation of January 1999. The global-mean lifetime of aerosols in the troposphere is ~5 days, and therefore the simulation of the PEM Tropics B flights is nearly independent of the initial conditions.

Note that all numerical methods, no matter how accurate, have difficulty resolving features with spatial extent less than three or four cells. Therefore we anticipate uncertainties with MATCH simulating features less than about two hundred kilometers wide in the horizontal or less than a hundred meters or so thick in the vertical near the surface, or a few hundred meters thick near in the middle troposphere. This means that plumes with fine spatial scales will be diffused somewhat and that the diffusion will increase as the plumes leave the source region. One should not expect to resolve the position of transition regions (e.g., between polluted and pristine regions) to better than 1 or 2 grid points (about two hundred km horizontally, or a few hundred meters vertically) [*Kalnay et al.*, 1996].

It is also instructive to place model behavior in the context of the three-dimensional air mass trajectories that they encompass. A sense of the trajectories involved is revealed in back trajectories from every 5 min of the stairstep trajectory (Fuelberg et al., this issue). These are shown in Plate 4 along with two locations displaced 200 km to the north and south in order to illustrate the spatial sensitivity consistent with the expected model uncertainties mentioned above both vertical and horizontal representations. There are a number of important features evident in the trajectories as we move back along them. First, a day or so before reaching our profile location, the westernmost trajectories reveal some tight cyclonic activity near 35N,145W (shown as 215E in Plate 4). These smaller features are not always well captured in the model products. As we continue back two or three more days, it is clear that trajectories go to 55N and ascend to the 400-600 mbar pressure altitudes. At ~50N and 180E the trajectories are spread greatly in the vertical, implying air mixed over a range of altitudes. This is evident in both the vertical and horizontal presentations where cyclonic activity is manifest near Japan at 35N, 155E. The reliability of the trajectories and vertical position upstream from this cyclonic activity is probably degraded since they do not capture rapid sub-grid scale vertical transport in convection associated with the cyclones.

Some trajectories encountered near 900 mbar on our stepped ascent show looping behavior consistent with passage through the cyclonic activity while others appear to be swept north around the system and over northern Japan. This system is part of the large scale cyclonic activity evident in the April 4 SeaWiFS image (Plate 1a). Farther to the west the vertical trajectory presentation shows a number of trajectories nearing the land surface at 40N, 100E. This is the south central Gobi Desert in China, a well-recognized source region for these types of dust events. Hence a number of back trajectories for our stairstep profile clearly suggest surface dust injection from the Gobi desert followed by cyclonic activity near southern Japan. This could mix dust with polluted low-level air from China, Korea, and Japan before being lofted to ~5 km for transport over the North Pacific prior to subsidence just above the marine inversion between Hawaii and California.

7. Model Results

Model products for the April 10 flight are shown in Plates 5a-5d. These present the modeled column aerosol optical depth (AOD) for sulfate (Plate 5a) and dust (Plate 5b), the two major contributors to AOD. Note that the model area influenced by dust is similar in shape and location to the dry area evident in the water vapor imagery (Plate 1c). Also shown are vertical cross sections of mass concentrations of these constituents in the model calculated along the actual aircraft flight track (Plates 5c and 5d). The stairstep ascent profile discussed above for the aerosol data is near the middle of the flight. Our ascent clearly intersects the model values for elevated aerosol concentrations between ~730 and 850 mbar. This occurs at the exact position of the elevated aerosol concentrations observed in our aircraft data as seen in the light scattering (Plate 2c) and size distribution data (Plate 2b). For the stairstep region the model AOD for sulfate lies in the 0.04±0.02 range and for dust lies in the 0.12±0.02 range (Figures 4a and 4b). The model also shows considerable coarse particle sea salt below ~1 km as was also inferred above in our discussion of Plate 2b. This will add ~0.02 to the column AOD and suggests a total column model AOD of 0.18±0.04 or so, most of which will be below our maximum aircraft altitude. These model values are somewhat lower than our estimate above determined from our in situ data (0.20±0.03) but lie within uncertainty estimates. The lower value is due primarily to an underestimate of the dust component (see below).

Model performance is also revealed when we compare model behavior with data collected along the 4000-km flight path and presented as a time series in Figure 4. To do this, we have taken the model sulfate and dust mass concentrations evident in Plates 5c and 5d and used representative values of light scattering to mass for the dry sulfate (3.3 m^2g^{-1}) [*Waggoner et al.*, 1981] and dust modes (0.7 m^2g^{-1}, as estimated from our measured size distributions). These were then multiplied by the modeled dry mass values along the path to obtain effective model dry scattering coefficients at 550-nm wavelength. The value of 3.3 m^2g^{-1} is consistent with optical properties that we use for sulfate. The estimate of 0.7 m^2g^{-1} for dust is probably a little low when applied to the model since nearly all of the model dust and modeled optical depth is in the submicron range, and the scattering to mass ratio for that range is closer to 1.3 m^2g^{-1}. This may contribute to some of the discrepancies evident for the dust layer at 1.5-2 km (see below). Even so, this approach provides a simple model estimate of fine and coarse dry aerosol scattering extinction that can be compared to the nephelometer dry light scattering data. Comparisons of this time series must be made in the context of the horizontal cross-section data (Plate 5) and previously discussed model uncertainties since regions of significant gradients are involved.

In view of model resolution discussed above, along with the modeled value of the total coarse and fine aerosol (sulfate, dust and sea-salt) contribution to scattering along the path, we have included maximum and minimum values expected if our path had been displaced 200 km to the north or south. This was done to provide a simple measure of model spatial uncertainty and is included as the gray shaded region in Figure 4a. A wider gray region indicates greater horizontal differences in modeled north-south aerosol concentrations across the flight path.

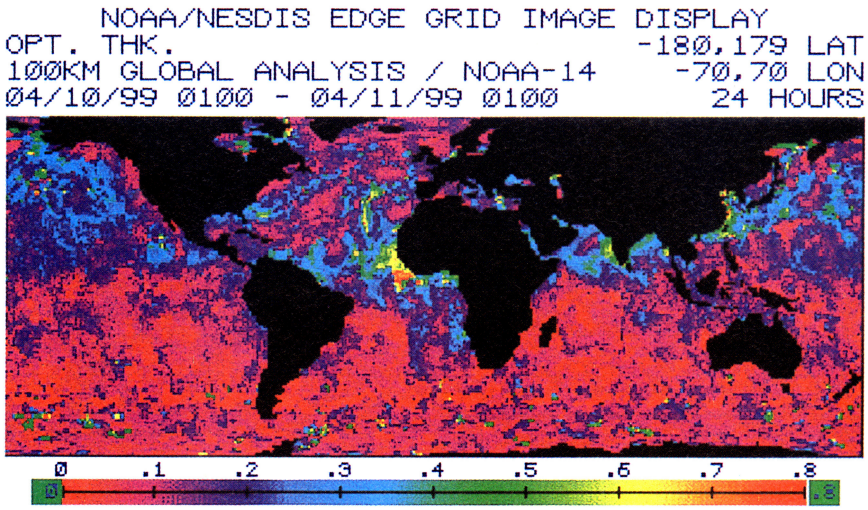

Plate 3. AVHRR optical depth image 100-km average for April 10 and 11. This image is only updated for clear regions for satellite overpasses so that most of the image is a "memory" of earlier days and satellite passes. Even so, the tendency for enhanced optical depth in the North Pacific is evident, and values between Hawaii and California are ~0.15–0.25 for this image.

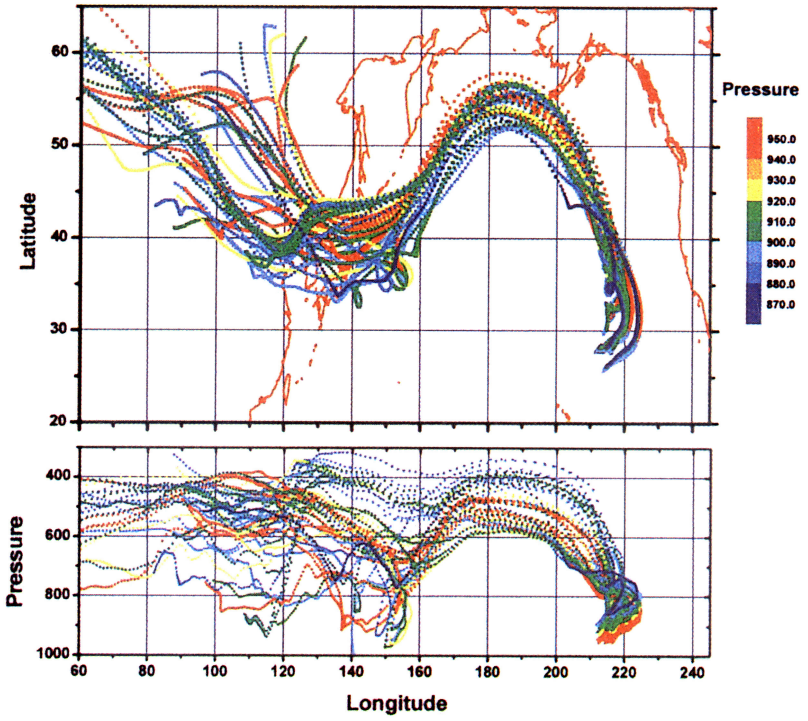

Plate 4. Ten-day back trajectories shown in horizontal (latitude, longitude) and vertical (pressure in mbar) projections for every 5-min flight interval of the stepped ascent region for flight 18. Trajectories are color coded for the pressure altitude they terminated on during the stepped ascent, as indicated in lower panel. Trajectories are also included for a location 200 km to the north and south of our location in order to gauge variability. Trajectories are back to the north at the same time they ascend to 400-600 mbar. Vertical motions indicate that many trajectories touch down in the vicinity of the cyclonic activity off Japan (Plate 1) and earlier over the southern Gobi desert.

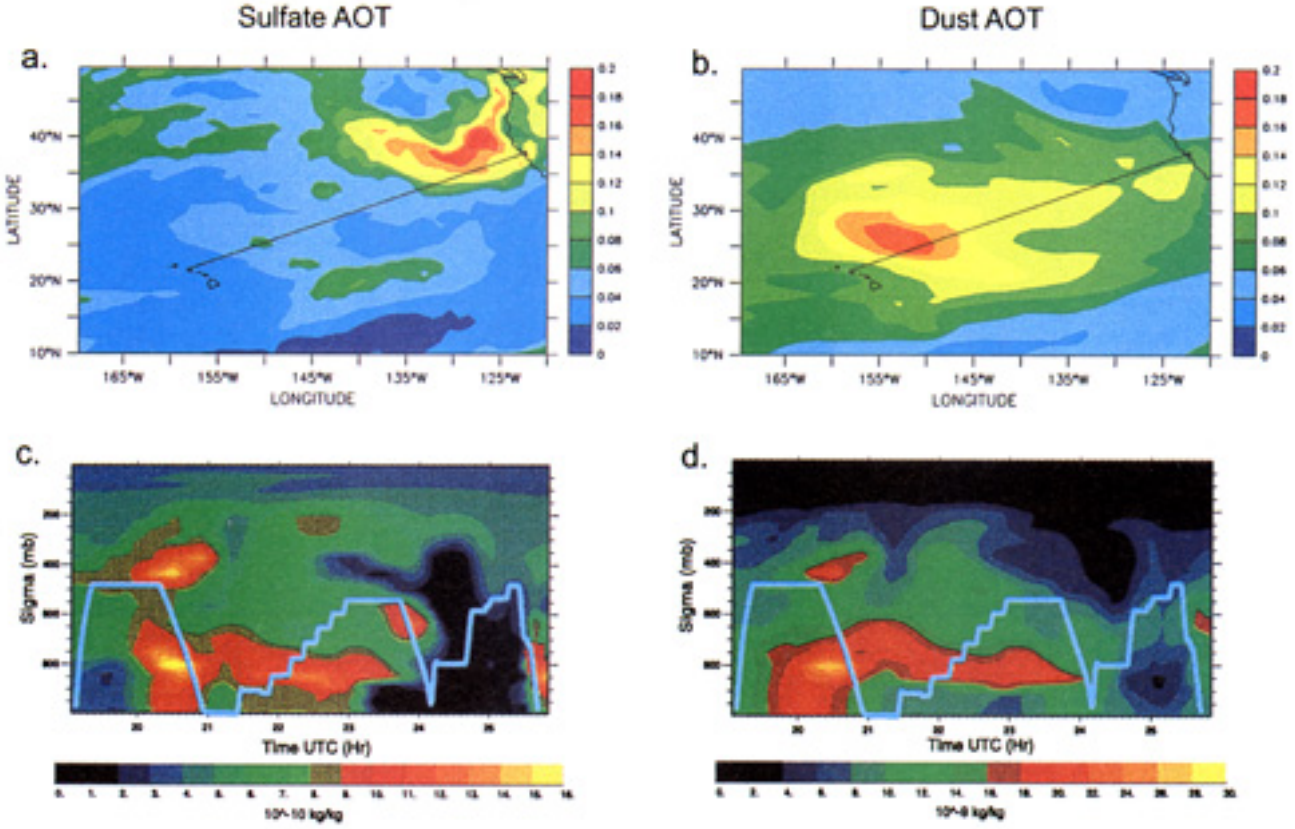

Plate 5. Model-predicted values of column optical depth due to (a) sulfate and (b) dust. Cross sections through the model are colocated with positions of our flight track (light blue) for (c) sulfate mass and (d) dust mass.

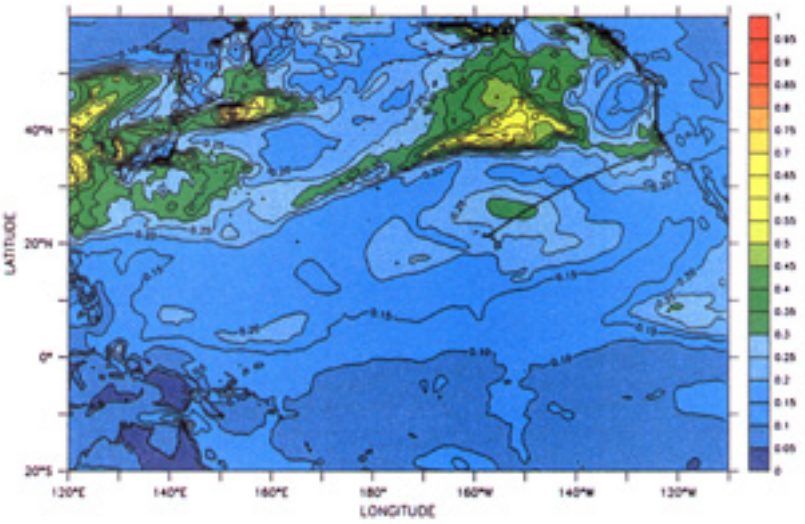

Plate 6. Model results over global scales for the same day evaluated in this paper. Note that the region between Hawaii and California is clearly impacted, but the more extended regions to the north have 2 to 3 times the AOD experienced during our flight 18.

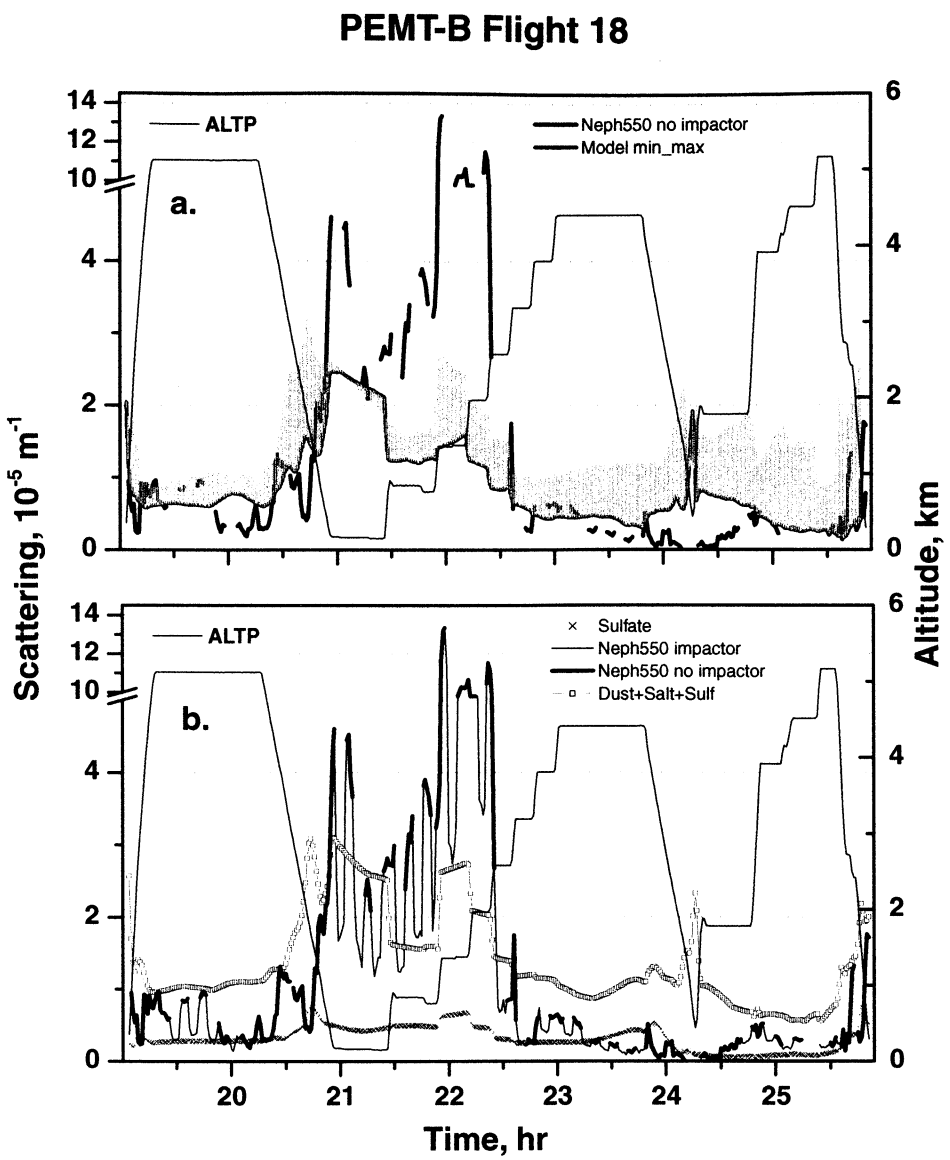

Figure 4. Time series comparison of measured and modeled optical properties based upon sulfate, dust, and sea-salt aerosol. Altitude profile (blue) reveals stairstep ascent near middle of flight. (a) Model mass values were used to generate associated light scattering coefficients (see text) for comparison to measured nephelometer scattering data. Model results are heavy gray line, and gray shading shows range of model values for flight tracks parallel to actual but displaced 200 km to north and to south as an estimate of model uncertainty (see text). Nephelometer scattering at 55 nm (magenta) is stratified to emphasize total scatter values (no impactor) and includes dust. (b) Here model inferred scattering for dust and sulfate for actual flight path are shown for clarity (no shaded uncertainty estimate as in Figure 4a). Nephelometer light scattering in Figure 4b includes the pronounced oscillation due to alternating between total and submicrometer scatter (thin line) with impactor (see text) such that minima should approach model sulfate scattering values when submicrometer dust or sea-salt contributions are small.

The nephelometer scattering extinction data are also generally cycled with a 1-μm impactor to distinguish between total and submicrometer scattering. When coarse particles are removed the scattering drops to values associated with the submicrometer aerosol often dominated by sulfates and soot (BC) along with the submicrometer tail of dust or sea salt when present (see Figure 3). In Figure 4a, only the total measured nephelometer scattering component has been retained for comparison to the model range of values. In Figure 4b the submicrometer scattering values are included in the nephelometer data as a thin line. Also shown are the model scattering values estimated from submicrometer sulfate and the total scattering estimated for the actual flight path.

Starting from the first ascent and initial horizontal leg until 19.8 hour, we see that peaks in measured scattering fall within the model range. This good agreement changes near 20 hour where the dust component is not evident in the cycled nephelometer data, but agreement remains between the nephelometer values and the model submicrometer sulfate as seen in Figure 4b. This difference in dust along the leg may be related to variations caused by the small scale cyclonic motion previously mentioned for the trajectory data that is not

well captured in the model. In the descent near 20.5 hour, again the model and dust scattering agree as we descend into a layer near 4 km (630 mbar, Plate 5c), but as descent continues, the measured scattering exceeds model estimates by 10 to 70%, although trends are similar. Minimum measured scattering values are also well above model fine aerosol sulfate, probably because enhanced submicrometer dust is also associated with these high dust values (see Figure 3). Measured scattering values continue to be higher than model estimates during the ascent and particularly in the region of peak dust. The dust layer location is very well resolved by the model (Plate 5d), but the measured light scattering near 2 km on the stepped ascent is ~3-4 times model dust scattering. Above 2 km the total light scattering values fall within the model range (Figure 4a) and submicrometer light scattering values are generally consistent with the model (Figure 4b) until ~23.5 to 24.5 hours. Here modeled total scatter is significantly larger than observed while sulfate values are variable but close to observed submicrometer scattering. Upon climbing to 4 km near hour 25 the total values and the submicrometer sulfate values fall within the model ranges and are in reasonable agreement. In the final descent near California the sulfate and dust increase in the model and their range again coincides with the measured scattering.

In this rather simple but stringent comparison of three-dimensional model performance the measured and model scattering extinction agree within the model variation more than 50% of the time in spite of a highly structured aerosol sampled at multiple altitudes over a 4000-km path. The largest disagreements are a model underestimate of the dust on the stairstep ascent and for the period centered around hour 24. In the first case we note that although significant dust concentrations with sizes clearly larger than 3 μm were observed (Figure 3), this model overestimates wet and dry removal of larger aerosol and is known to underestimate transport of dust with diameters above 2 μm more than 1000 km from the continents (P.J. Rasch, personal correspondence, 2000). This will lead to greater underestimates of the dust contributions for the larger dust events. The second region of largest disagreement is associated with the altitudes below 2 km centered near hour 24 where the model overpredicts both dust and sulfate scattering. This is the region of most active cloud in the visible imagery and high water vapor images (Plates 1b and 1c) and included deepest convective activity and high cloud in the IR imagery for this transect (Fuelberg et al., this issue). Here the in situ measurement with the aircraft Gerber probe also registered continuous liquid water (~0.6 g kg^{-1}) during the descent between 1.5 and 0.2 km after hour 24 when sustained rain was also reported from the cockpit. This is therefore a region of deep convection and precipitation that should result in strong aerosol removal and pumping of cloud scavenged air aloft. This would be consistent with the low measured aerosol volume and light scattering values both near the surface and aloft. Reconstruction of the 3-D precipitation field from NCEP analysis showed clouds a little to the north but no convective or large-scale precipitation in the area where it was observed by the aircraft . Hence aerosol removal through precipitation and vertical mixing of cloud scavenged air would be not represented in the model. This would account for the higher model aerosol concentrations than we observed in this region.

In view of these considerations it is evident that much of the complex structure characterized by the in situ aerosol measurements made during this flight is captured in the model. Here we have focused on the 4000-km region between Hawaii and California. However, model results for the same day (Plate 6) over the extended North Pacific reveal more extensive areas of more intense dust/pollution transport that puts our flight 18 region in context. In fact, on the previous day, a major plume event was also sampled by aircraft off the coast of Washington (D.A. Jaffe, personal correspondence, 2000). At this time of year the common occurrence of such events has been recognized by long-term light scattering and other measurements made at Mauna Loa Observatory, Hawaii [*Bodhaine*, 1995], and more recently in data collected off the Washington coast [*Jaffe et al.*, 1999] as well as by satellite products such as the multi-day composite in Plate 3. Therefore models provide a means to assess important characteristics related to their sources, composition, vertical structure, transformations of the aerosol, etc. As mentioned in the introduction, some of these features are critical to the assessment of issues involving atmospheric chemistry and global change such as the direct and indirect forcing of natural and anthropogenic aerosol.

One particular issue that is confirmed by this study is the model prediction and clear in situ evidence for the long-range transport of pollution/dust aerosol penetrating the tradewind inversion (see Plate 2a). This implies that this enhanced accumulation mode aerosol is certain to contribute significantly to cloud condensation nuclei activated in MBL clouds, including the stratus common off the California coast and evident in Figure 2b. The size, concentration, and composition of this aerosol are very similar to the accumulation mode aerosol we have observed from natural and industrial combustion emissions (K. Moore et al., unpublished manuscript, 2001), both of which have been recently demonstrated to suppress precipitation from clouds downwind of such sources [*Rosenfeld*, 1999,2000]. The frequent occurrence of cross-Pacific aerosol transport events in the spring and this evidence for subsidence and entrainment through the inversion suggest that this condition is not uncommon. Hence there is reason to expect that this mechanism for rainfall suppression could also be possible elsewhere after over 10,000 km of transport downwind of the continents. Clearly, this is an example of how aerosol impacts could be expressed on global scales and examined through global CTM models.

8. Summary

In situ measurements of aerosol and gas over the central Pacific provided clear confirmation of the 3-D river-like transport of Asian dust and pollution over scales exceeding 10,000 km. Back trajectories confirmed the complex dynamics that influence this transport. Even so, well-defined horizontal and vertical structure was preserved and identified both in the data and the model products. Differences in aerosol intensive properties such as $\bar{\omega}$ were evident with upper plumes that had more soot relative to dust having $\bar{\omega}$ near 0.9, while lower plumes with more dust had values near 0.95. This indicates that the dust has a proportionally greater contribution to scattering than to absorption and that the soot component dominates the absorption characteristics. This and the measured dust contribution to scattering (Dp>1 μm) with and without an impactor (Plate 2c) suggests that $\bar{\omega}$ for the dust component ($\bar{\omega}_{dust}$) alone is about 0.97±0.01 and that lower values for the total aerosol are due to light absorbing BC from com-

bustion present in the submicrometer sizes. This value is consistent with our earlier measurements in the Pacific free troposphere where $\bar{\omega}$ averaged about 0.93±0.04 and $\bar{\omega}_{dust}$ averaged about 0.98±0.01 for more than 100 nightly measurements at Mauna Loa Observatory, Hawaii [*Clarke and Charlson*, 1985]. It is also similar to recent values of $\bar{\omega}_{dust}$ = 0.97±0.02 inferred from satellite [*Kaufman et al.*, 2001] for Saharan dusts. However, these values of $\bar{\omega}_{dust}$ are far greater (lower absorption) than values recently reported as representative of various models ($\bar{\omega}_{dust}$= 0.85 with range 0.65-0.95) [*Sokolik and Toon*, 1996] and suggest overestimates of dust absorption properties in many of these models.

The aerosol optical properties and the optical depth derived from the aerosol microphysics and chemistry usually agreed within ~25% of measured optical properties and provided an opportunity to interpret satellite and model behavior in terms of size resolved characteristics. Agreement with satellite AOD was within the uncertainty of the daily satellite average values for our flight path of ~0.15-0.25. Model column optical depths of 0.04±0.2 for sulfate and 0.12±02 for dust agreed favorably with our microphysics assessment of 0.04±0.2 and 0.16±0.2, respectively, but we observed greater dust concentrations in the layer during the stepped ascent.

Also, the contribution of coarse particles to measured extinction in the layer was ~60% of the total, as evident in the impactor data (Plate 2c, Figure 4b). This is consistent with the coarse particle size distribution data and is much more than is present in the model which for this region had most of the dust mass in the submicrometer mode. Refinements in the model dust parameterization including the dust source and transport algorithms are underway.

We note that in spite of the strong influence on the light scattering coefficient by the coarse dust, the number distribution (Plate 2a) is actually dominated by the submicrometer fine mode that includes the soot, sulfate, and other combustion constituents. This aerosol was concentrated in a layer just above the inversion (1.3 km) and demonstrated to be entraining into the MBL from aloft. This type of combustion aerosol is very similar to those recently shown to have dramatic influence on suppressing rainfall [*Rosenfeld*, 1999,2000]. This pronounced layer lies immediately above the altitudes common to California stratus (Plate 1b) and could be expected to play a similar role in drizzle suppression and cloud lifetime enhancement over extended regions of Pacific. Hence, during periods of enhanced long range pollution transport aloft followed by entrainment and mixing into the MBL, it appears possible that cloud physical, chemical and optical properties could be perturbed by sources 10,000 km or more distant.

The observations, trajectories, and model outputs discussed here clearly demonstrate that aerosol and gaseous emissions must generally be viewed as three-dimensional rivers of material that stretch and distort during their transport. In spite of complex vertical mixing, transport, and subsidence, the new generation of model described here has tight coupling to well-resolved meteorological fields and appears able to capture the highly structured features of this transport. It provides qualitative and reasonably quantitative assessments of key physical, chemical, and optical properties of the aerosol.

At present no information is used to help the model infer aerosol composition or constrain the aerosol vertical distribution. Consequently, the assimilation adjusts all aerosol types uniformly in the vertical. In the future it is planned to utilize observations (multispectral measurements of aerosol properties and lidar data that provide information on the vertical distribution of the aerosols) as they become available. Even so, we feel this first-time validation of an aerosol model with very long-range transport in the free troposphere indicates promise of these new generation models to address current issues. It also suggests that similar models might be used as a tool to complement and extend satellite data products for regions of sparse coverage or regions obscured by cloud. The detailed models can, in essence, be viewed as a physically based method for interpolating satellite data onto a regular space-time grid or as a method for placing these data in a global analytical context. There remains a clear need for more systematic comparison studies of this kind over extended regions.

Acknowledgments. The authors wish to thank the crew and personnel of the NASA P3 aircraft and GTE project staff for their help and cooperation during PEM Tropics B. We are also grateful for the support provided by the National Aeronautic and Space Administration Global Tropospheric Experiment under grant NCC-1-315 and the scientific guidance of Joe McNeal and Jim Hoell. Other contributions to this analysis effort were supported under NASA grant NAG5-8118. Model activities were supported in part by NASA grant MTPE S-97889-F (WDC) and NSF award ATM9405024 to the Center for Clouds, Chemistry, and Climate (PJR). We also thank Brian Eaton (NCAR) for his role in preparing and running the global aerosol assimilation for the model. SOEST contribution 5843.

References

Ackerman, A., O.B. Toon, D.E. Stevens, A.J. Heymsfeld, E.J. Welton, and V. Ramanathan, Reduction of tropical cloudiness by soot, *Science, 288*, 1042-1047, 2000.

Albrecht, B., Aerosols, cloud microphysics and fractional cloudiness, *Science, 245*, 1227-1230, 1989.

Anderson, T.L., and J. Ogren, Determining aerosol radiative properties using the TSI 3563 integrating nephelometer, *Aerosol Sci. Technol., 29*, 57-69, 1998.

Blanchard, D.C., and A.H. Woodcock, Production, concentration, and vertical distribution of the sea salt aerosol, *Ann. N.Y. Acad. Sci., 338*, 330-347, 1980.

Bodhaine, B.A., Aerosol absorption measurements at Barrow, Mauna Loa and the South Pole, *J. Geophys. Res, 100*, 8967-8975, 1995.

Charlson, R.J., S.E. Schwartz, J.M. Hales, R.D. Cess, J.A. Coakley Jr., J.E. Hanse, and D.J. Hofmann, Climate forcing by anthropogenic aerosols, *Science, 255*, 423-430, 1992.

Chowdhury, Z., L.S. Hughes, L.G. Salmon, and G.R. Cass. Atmospheric particle size and composition measurements to support light extinction calculations over the indian ocean. In press, *J. Geophys. Res.*, 2001.

Clarke, A.D., Aerosol light absorption by soot in remote environments, *Aerosol Sci. Technol., 10*, 161-171, 1989.

Clarke, A.D., A thermo-optic technique for in-situ analysis of size-resolved aerosol physicochemistry, *Atmos. Environ., Part A, 25*, 3/4, 635-644, 1991

Clarke, A.D., A global survey of atmospheric nuclei in the remote mid-troposphere: their nature, concentration and evolution, *J. Geophys. Res, 98*, 20,633-20,647, 1993.

Clarke, A.D., and R.J. Charlson, Radiative properties of the background aerosol: Absorption component of extinction, *Science, 229*, 263-265, 1985.

Clarke, A.D., J.N. Porter, F. Valero, and P. Pillewski, Vertical profiles, aerosol microphysics and optical closure during ASTEX: Measured and modeled column optical properties, *J. Geophys. Res., 101*, 4443-4453, 1996.

Clarke, A.D., T. Uehara, and J.N. Porter, Atmospheric nuclei and related aerosol fields over the Atlantic: Clean Subsiding Air and Continental Pollution during ASTEX, *J. Geophys. Res., 102*, 25,821-25,292, 1997.

Clarke, A.D., J.L. Varner, F. Eisele, R. Tanner, L. Mauldin, and M. Litchy, Particle production in the remote marine atmosphere:

Cloud outflow and subsidence during ACE-1, *J. Geophys, Res., 103*, 16,397-16,409, 1998.

Clarke, A.D., F. Eisele, V.N. Kapustin, K. Moore, R. Tanner, L. Mauldin, M. Litchy, B. Lienert, M.A. Carroll, and G. Albercook, Nucleation in the equatorial free troposphere: Favorable environments during PEM-Tropics, *J. Geophys. Res., 104*, 5735-5744, 1999.

Clarke, A.D., S. Howell, P.K. Quinn, T.S. Bates, E. Andrews, A. Jefferson, and J.A. Ogren, The INDOEX aerosol: A comparison and summary of microphysical, chemical, and optical properties observed from land, ship, and aircraft, *J. Geophys. Res.*, in press, 2001.

Collins, W.D., P.J. Rasch, B.E. Eaton, B.V. Khattatov, J. F. Lamarque, and C.S. Zender, Simulating aerosols using a chemical transport model with assimilation of satellite aerosol retrievals: Methodology for INDOEX, *J. Geophys. Res., 106*, 7313-7336, 2001.

Cooke, W.F., and J.N. Wilson, A global black carbon aerosol model, *J. Geophys. Res, 101*, 19,395-19,409, 1996.

Duce, R.A., and N.W. Tindale, Atmospheric transport of iron and its deposition in the ocean, *Limnol. Oceanogr., 36*(8), 1715-1726, 1991.

Fuelberg, H., R.E. Newell, D.J. Westberg, J.C. Malonay, J.R. Hannan, B.C. Martin, and Y. Zhu, A meteorological overview of the second Pacific Exploratory Mission in the Tropics, this issue.

Galloway J.N., R.J. Charlson, M.O. Andreae, and H. Rodhe, *The Biogeochemical Cycling of Sulfur and Nitrogen in the Remote Atmosphere*, D. Riedel, Norwell, Mass., 1984.

Jaffe D.A., et al., Transport of Asian air pollution to North America, *Geophys. Res. Lett., 26*, 711-714, 1999.

Kalnay, E., et al., The NCEP/NCAR 40-year reanalysis project, *Bull. Am. Meteorol. Soc., 77*, 437–471, 1996.

Kaufman, Y., and R. Fraser, The effect of smoke particles on clouds and climate forcing, *Science, 277*, 1636-1639. 1997.

Kaufman, Y., D. Tanre, O. Dubrovik, A. Karnieli, and L. Remer, Absorption of sunlight by dust as inferred from satellite and ground-based remote sensing, *Geophys. Res. Lett., 28*, 1479–1482, 2001.

King, M.D., Y.J. Kaufman, D. Tanre, and T. Nakajima, Remote sensing of aerosol from space: Past, present and future, *Bull. Am. Meteorol. Soc., 80*, 2229–2259, 1999.

Liousse. C., F. Dulac, H. Cachier and D. Tanre, Remote sensing of carbonaceous aerosol production by African savanna biomass burning, *J. Geophys. Res., 102*, 5895–5911, 1997.

Martin J.H., and R.M. Gordon, Northeast Pacific iron distributions in relation to phytoplankton productivity. *Deep-Sea Res., 35*, 177–196, 1987.

Massling, A., A. Wiedensohler, B. Busch, C. Neusuess, P. Quinn, T. Bates, and D.S. Covert. Hygroscopic properties and solubility of different aerosol types over the Indian Ocean. In press, *J. Geophys. Res.*, 2001.

Measures, C., and S. Vink, On the use of dissolved aluminum in surface waters to estimate dust deposition to the oceans, *Global Biogeochem. Cycles, 14*, 317–327, 2000.

Penner, J.E., H. Eddleman, and T. Novakov, Towards the development of a global inventory for black carbon emissions, *Atmos. Environ., 27*, 1277–1295, 1993.

Parungo, F., Y. Kim, J. Harris, X. Li, M. Z. Chen, and K. Park, Asian duststorms and their effects on radiation and climate, *Tech. Rep. 2906*, STC Corp., Hampton Va., 1995.

Porter, J.N., A.D. Clarke, R. Peuschel, G. Ferry, and B.J. Huebert, Aircraft studies of size-dependent aerosol sampling through inlets, *J. Geophys. Res., 97*, 3815–3824, 1992.

Prospero, J.M., Long-term measurements of the transport of African mineral dust to the southeastern United States: Implications for regional air quality, *J. Geophys. Res., 104*, 15,917–15,927, 1999.

Quinn, P.K., S.F. Marshall, T.S. Bates, D.S. Covert, and V.N. Kapustin, Comparison of measured and calculated aerosol properties relevant to the direct radiative forcing of sulfate aerosols on climate, *J. Geophys. Res., 100*, 8977–8991, 1995.

Rasch, P.J., N.M. Mahowald, and B.E. Eaton, Representations of transport, convection, and the hydrologic cycle in chemical transport models: Implications for the modeling of short-lived and soluble species., *J. Geophys. Res., 102*, 28,127–28,138, 1997.

Rasch, P.J., W.D. Collins, and B.E. Eaton, Understanding the Indian Ocean experiment INDOEX aerosol distributions with an aerosol assimilation, *J. Geophys. Res., 106*, 7337–7355, 2001.

Rosenfeld, D. TRMM Observed first direct evidence of smoke from forest fires inhibiting rainfall, *Science, 26*, 3105–3108, 1999.

Rosenfeld, D., Suppression of rain and snow by urban and industrial air pollution, *Science, 287*, 793–796, 2000.

Sloane, C.S., Optical properties of aerosols of mixed composition, *Atmos. Environ., 4*, 871–878, 1984.

Smith, S.J., H. Pitcher and T.M.L.Wigley, Global and regional anthropogenic sulfur dioxide emissions, *Global Biogeochem. Cycles, 29*, 99–119, 2001.

Sokolik, I., and O. Toon, Direct radiative forcing by anthropogenic airborne mineral aerosol, *Nature, 381*, 681–683, 1996.

Stowe, L.L, A.M. Ignatov, R.R. Singh, Development, validation, and potential enhancements to the second-generation operational aerosol product at the National Environmental Satellite, Data, and Information Service of the National Oceanographic and Atmospheric Administration, *J. Geophys. Res., 102*, 16,889–16,910, 1997.

Tang, I.N., A.C. Tridico, and K.H. Fung. Thermodynamic and optical properties of sea salt aerosols. *J. Geophys. Res. 102*, 23,269-23,275, 1997.

Tegen, I., P. Hollrig, M. Chin, I. Fung, D. Jacob. and J. Penner, Contribution of different aerosol species to the global aerosol optical thickness: estimates from model results, *J. Geophys. Res., 102*, 23,895–23,915, 1997.

Waggoner, A.P., R.E. Weiss, N.C. Ahlquist, D.S. Covert, S. Will, and R.J. Charlson, Optical characteristics of atmospheric aerosols, *Atmos. Environ., 15*, 1891–1909, 1981.

A. D. Clarke, S. Howell, V. N. Kapustin, and K. Moore, School of Ocean and Earth Science and Technology, 1000 Pope Road, MS 8502, University of Hawaii, Honolulu, HI 96822 (tclarke@soest.hawaii.edu)

W. G. Collins and P. J. Rasch, National Center for Atmospheric Research, Boulder, CO 80305.

H. E. Fuelberg, Department of Meteorology, Florida State University, Tallahassee, FL 32306.

(Received August 29, 2000; revised December 1, 2000;
accepted December 5, 2000.)